Journal of Electrostatics 96 (2018) 85–89

Contents lists available at ScienceDirect

Journal of Electrostatics

journal homepage: www.elsevier.com/locate/elstat

Ultra near-field electrohydrodynamic cone-jet breakup of self-reducing silver inks

Christopher S. Lefky[a], Avinash Mamidanna[b], Owen J. Hildreth[b,*]

[a] Arizona State University, School for Engineering Matter, Transport, and Energy, Tempe, AZ, 85287, USA
[b] Colorado School of Mines, Department of Mechanical Engineering, Golden, CO 80401, USA

ARTICLE INFO

Keywords:
Reactive ink
Silver
Electrohydrodynamics
Cone-jet

ABSTRACT

Ultra near-field electrohydrodynamic (UNF-EHD) jetting of highly conductive self-reducing silver inks is investigated and compared to a theoretical cone-jet breakup model. While models connecting spray angle to fluid properties exist for large substrate-nozzle gap and inks with high ionic conductivity, little is known about the validity of these models when operating under UNF conditions. Using a pulsed cone-jet approach, data on the effects of nozzle height, applied voltage, and waveform (pulse length, pulse frequency, number of pulses/bursts, and delay between bursts) on spot size were collected showing high conductivity inks have a feature resolution very dependent on substrate-nozzle gap.

1. Introduction

Electrohydrodynamic (EHD) jetting is a robust, electric-field driven technique with numerous uses including thin film deposition [1], nanoparticle synthesis [2], and processing living organism suspensions [3]. In this process, liquid is dispensed from a capillary under application of a large electric field. Depending on fluid properties, applied electric field strength, and capillary shape, various flow regimes [4–6] can be accessed to create individual droplets from nm to mm in diameter [7], long fibers [8,9], or atomize fluids [10,11]. Of the numerous fluid properties that impact flow regime, fluid conductivity is closely tied to both the accessibility of different regimes [12] along with the stability of the jet [13]. Specifically, studies have shown that Coulombic repulsion and jet destabilization increases as fluid conductivity increases, with complete jet destabilization occurring as fluid conductivity exceeds approximately 10^{-3} S/m [14,15].

To avoid jet destabilization and improve feature resolution, most EHD inks consist of polymers [16] or colloidal nanoparticle solutions [6,14] dispersed in a non-polar solvent. While the nanoparticle inks have their utility fabricating plasmonic structures [17] or ultra-fine electrical interconnects [18], the net result of these dispersions is a cluster of particles that require additional thermal annealing to improve their mechanical and electrical properties [19]. Some of these inks can be susceptible to oxidation [20]; however, low temperature Ag nanoparticle inks [21] have been developed without significant oxidative issues [22]. Replacing particle-based inks with self-reducing reactive inks has the potential to eliminate the annealing step while also improving material properties. These inks are often easier to synthesize than nanoparticle-based inks [23] and low temperature reactive inks have been developed for Ag [23], Cu [24], and Al [25,26] that can deposit reasonably pure metals at temperature below 150 °C and with electrical properties close to those of bulk materials.

The limited research on EHD printed reactive inks largely focuses on very dilute reactive inks with very low conductivity (10^{-8} S/m–10^{-6} S/m) [27] and no information exists on the behavior of concentrated reactive inks where the high concentration of polar reactants and ionic species increases the conductivity of the ink to the point that Coulombic repulsion causes early jet destabilization [13]. In this study, the relationships between substrate-to-nozzle separation distance in the ultra-near field (UNF), applied voltage, electric field strength, and spot size were determined to show that an existing model for electrospray cone-jet breakup [13] accurately predicts the plume angle for reactive inks even in the ultra near-field condition. Our results verify that Coulombic fission occurs almost immediately as the fluid exits the nozzle with spray angle increasing with increasing electric field strength. This is in sharp contrast to the nano-drip EHD regime accessible to low-conductivity fluids, where droplet size is nearly independent of small changes in nozzle heights [6]. While neither the micro-drip or nano-drip regime could be accessed for the self-reducing silver ink used in this study, we do show that fluids with a high electrical conductivity can still be used to deposit fine features consisting of self-reducing ink even as it sprays with a 40° cone angle.

* Corresponding author.
E-mail address: ohildreth@mines.edu (O.J. Hildreth).

https://doi.org/10.1016/j.elstat.2018.10.006
Received 6 October 2018; Accepted 8 October 2018

Overall, this work demonstrates the ability to use a self-reducing, reactive silver ink [23] in the EHD cone-jet regime to deposit spots down to 5 µm in outer diameter. A Coulombic repulsion model for jet breakup was validated to explain relationships between fluid properties, applied voltage, nozzle height, and observed outer spray diameter.

2. Experimental methods

2.1. Ink synthesis

The room temperature, self-reducing silver reactive ink detailed by Walker et al. was used as a starting point for the reactive ink used in this study [23]. In this study, silver nitrate was used instead of silver acetate to increase the reduction temperature of the ink and reduce nozzle clogging without having to overly dilute the ink. All chemicals were used as received. 2.00 g of silver nitrate ($C_2H_3AgO_2$; anhydrous 99%, *Alfa Aesar*) was dissolved in 5.00 mL of 35 wt% ammonium hydroxide (NH_4OH; ACS grade, *BDH Chemicals*). The solution was then stirred for 2 min on a vortex mixer. 0.40 mL of formic acid (CH_2O_2; ≥96%, *Sigma Aldrich*) was added in two steps with a quick stir at the end of each step. The ink was then allowed to sit for 12 h before being filtered through a 450 nm nylon filter and stored in the dark at 3 °C until use. For printing, the ink was diluted with 2,3-butanediol (BD, $C_4H_{10}O_2$, 98%, *Alfa Aesar*) at a volumetric ratio of 1:200 base Ag ink:BD (0.11 wt% Ag) to improve the stability of the ink for inkjet printing. An ink dilution, coupled with a hydrophobic layer at the capillary tip (discussed below), greatly reduces clogging, allowing for prints lasting on the order of hours even with the nozzle held 2 µm above a 72 °C heated substrate. Fluid conductivity was measured after ink preparation with a conductivity probe (SevenExcellence, *Mettler Toledo*).

2.2. Jetting process

Thin walled 750 µm inner diameter (ID) glass capillaries (TW100F-4, *World Precision Instrument)* were pulled to IDs ranging from 1 to 2 µm using a four-step micropipette puller (PUL-1000, *World Precision Instruments*). Approximately 10 nm of gold was deposited using a DC sputter coater (108 Auto Sputter Coater, *Ted Pella*). A n-type single-sided silicon wafer substrate was used with a 50.8 mm diameter, ⟨100⟩ orientation, 0.001–0.005 Ω-cm resistivity, and 280 µm thickness (ID 2270, *University Wafer*). The capillary tip and substrate were dipped in 0.1 wt% 1H,1H,2H,2H-per-fluorodecane-1-thiol ($C_{10}H_5F_{17}S$, 97%, *Sigma Aldrich*) in dimethylformamide (C_3H_7NO, ≥99.8%, *Sigma Aldrich*) for 12 min to form hydrophobic layers with a 3 min anneal at 100 °C to drive off residual solvent [15]. A nozzle is then loaded with approximately 5 µL of the diluted reactive ink using a stainless steel dispensing needle (6710A38, *McMasterCarr*) and positioned over a substrate. No fluid delivery system was used during loading or printing to increase the flow rate or apply a specific pressure. To avoid damaging the tip prior to printing, the approximate substrate nozzle separation was determined using an optical microscope. The actual nozzle height was determined at the end of the print by incrementally moving the substrate upwards towards the nozzle (40 nm/increment) while monitoring the electrical resistance between the nozzle and the substrate. The nozzle height was set to 0 µm once the resistance dropped below 10,000 Ω. To ensure that any x/y movements were accurate, it is necessary to take into account that the substrate will not be perfectly flat. An optical displacement sensor (ZW-Series, *Omron*) was used to measure the height at four different locations on the substrate, all spaced 5 mm apart. From these measurements dz/dx and dz/dy were calculated such that for any movement in x/y, the nozzle height would be adjusted to account for the slope of the substrate.

A pulsed, square-wave voltage signal was applied between the pipette and substrate using a signal generator (33510B Waveform Generator, *Keysight*) connected to a high-speed, high-voltage amplifier (10/10B-HS High Voltage Amplifier, *Trek*). The rise and fall times of the output amplifier waveform were measured using an oscilloscope (DSO-X 3024A, *Agilent Technologies*). A schematic of the waveform used in this study is shown in Fig. 1 that consisted of a burst of pulsed square waves with a wait time between each set of pulses. For each substrate-nozzle separation tested, 100 V was chosen as the starting voltage, and it was increased in increments of 10 V. This allowed all tests to begin at approximately the turn-on voltage. The nozzle was held stationary while the substrate position was controlled using a *Newport* 8-axis Universal Controller/Driver connected to a custom 3-axis stage (xyz) setup. An image of the EHD setup is annotated in Figure S1.

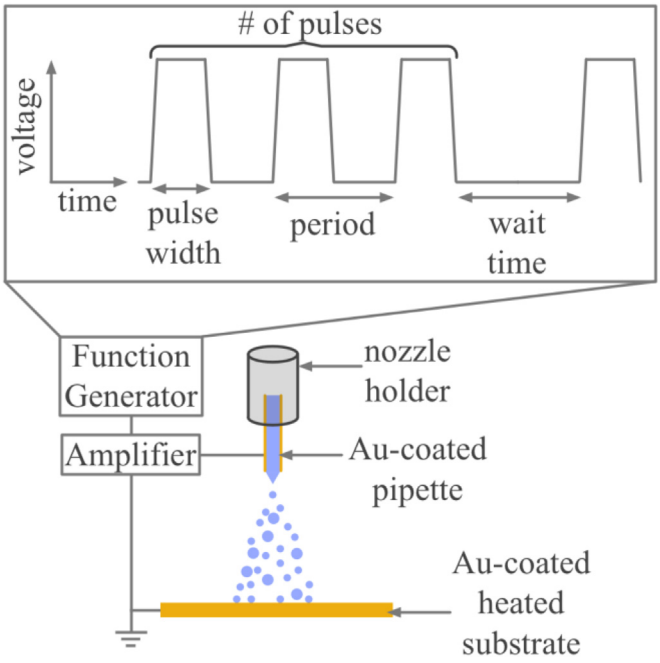

Fig. 1. Schematic of the experimental setup using a pulsed voltage to emit a spray of droplets. The input waveform consisted of a number of pulses followed by a wait time. The amount of pulses/burst was selected such that an observable amount of material was deposited. A wait time was used to ensure that adequate drying time was provided to ensure accurate spot size measurements.

The substrate was kept at 72 °C to ensure that solvent evaporation occurred before subsequent bursts were deposited and allow for faster deposition times. Additionally, the nozzle was regularly purged approximately every 5 min for 10 msec at 1000 V with a nozzle height of 200 µm.

2.3. Characterization

Morphology was characterized using an Amray 1910 Field Emission Scanning Electron Microscope (FESEM) at 20 kV accelerating voltage and a working distance of 5 mm for top-down images. An Apollo XPP Energy Dispersion Spectrometer (EDS) operating at 20 kV was used to collect spectra of a printed dot.

3. Results and discussion

As liquid conductivity increases, the EHD nano-drip, micro-drip, and dripping regimes associated with low flow rates and low electric field strengths are no longer accessible [14,16,17]. In this work, we modified the self-reducing silver reactive ink developed by Walker et al. to work with ultra near-field EHD jetting to deposit solid silver 2D dots with diameters down to 5 µm despite cone-jet breakup. Specifically, the silver acetate was replaced with silver nitrate and the dilution levels were increased to 200:1 (2,3-butanediol:base silver ink). These changes keep the reactive silver ink from reducing and clogging the 1 µm nozzles used in this study. Even when diluted 200:1, the ammonia and

silver salt-based reactive inks used in this study have ionic conductivities greater than 0.02 S/m. This is above the 10^{-3} S/m conductivity limits associated with the EHD nano-drip, micro-drip, and dripping regimes [14,16,17]. Instead, the pulsed cone-jet approach (see Fig. 1; not to be confused with the EHD pulsating regime) [30–33] was used to control the amount of ink deposited. Since no literature exists on the behavior of inks with high conductivities in the ultra near-field regime (nozzle height less than 10 µm), an initial parameter space investigation was conducted to establish a set of waveform parameters that balanced silver deposition rate (higher is better) with solvent evaporation time (smaller is better) while also avoiding nozzle clogging. The final printing parameters were selected to give the smallest observable diameter under the assumption that larger deposits were due to the printed ink not fully drying between bursts. Although most experiments lasted less than 2 h, a longer stability time ensured that any observed differences are due to varying the parameters, and not due to silver accumulation at the nozzle tip. Energy Dispersive Spectroscopy (EDS) of a deposited spot is seen in Figure S2 verifying that the printed features are silver.

The pulse width, pulse frequency, and number of bursts were selected such that a visible amount of material is observed under an optical microscope and SEM. A hydrophobic substrate was used to ensure accurate measurements of the plume angle (spreading of droplets on a hydrophilic surface would cause an overestimate). We chose a pulse frequency of 100 Hz (see Figure S3 in Supporting Information), a pulse width of 50 µs (see Figure S4 in Supporting Information), a pulse number of 10 pulses/burst and a wait time between bursts of 2 s. Figure S4 plots observed outer spot size vs. voltage for various pulse widths at a substrate-nozzle separation of 5 µm. The decrease in spot size with pulse width could be due to several factors. First, the amount of ink ejected from the nozzle decreases with decreasing pulse width and the decrease in spot size could suggest that the low vapor pressure ink has time to spread and is not fully evaporating until the pulse width is reduced to 5 µs? Second, the actual waveform is not a perfect square wave and our setup had a measured rise and fall time of 7 µs each for a 50 µs, 200 V pulse. The percentage of the waveform that reaches the peak applied voltage decreases significantly as the pulse width drops below 25 µs (e.g. 72% at 50 µs, 70% at 25 µs and 45% at 10 µs for 200 V; see Figure S5 in Supplementary Information). Ultimately, a pulse width of 50 µs was selected because it provided consistent results between samples; however, the results in Figure S4 do suggest that finer features could be achieved with shorter pulses.

A spot-to-spot spacing of 25 µm was chosen to ensure that there was no overlap between spots. Figure S6 shows ~4 µm outer diameter spots printed with a substrate-nozzle separation of 2 µm and a spot-to-spot spacing of 5 µm. Despite the decreased spacing between spots, there is no observable effect on the morphology or shape.

Fig. 2 shows representative SEM data for nozzle heights of 2 µm and 5 µm with applied voltages of 200, 210 and 220 V. Figure S7 in Supplementary Information shows representative images for voltages and nozzle heights ranging from 200 to 250 V and 2–10 µm respectively. The diameter of the reduced silver (bright white structure) and the outer ring (slightly darker region surrounding the deposited silver) show the full area the reactive ink was sprayed over. Notice that for larger substrate separations, secondary spots begin to form. This is caused by satellite droplets that occur during the breakup process at greater flow rates [34]. The satellite breakup could possibly be avoided by increasing the viscosity [35].

Fig. 3 graphs the measured outer and crystallite spot sizes at various nozzle heights as nominal electric field strength is varied. The x-axis was set to electric field strength instead of voltage (as most EHD-related work) because the range in nozzle height varied by a factor of five, resulting in electric field strengths varying by an order of magnitude even though the applied voltage range was relatively narrow, from 170 V to 270 V. For this work, the nominal electric field strength is simplified to $E = V/h$, where V is the applied voltage difference between the nozzle and the substrate and h is the nozzle height above the substrate; this simplification ignores possible changes in the electric field strength due to material buildup and it does not consider the nozzle geometry of this system.

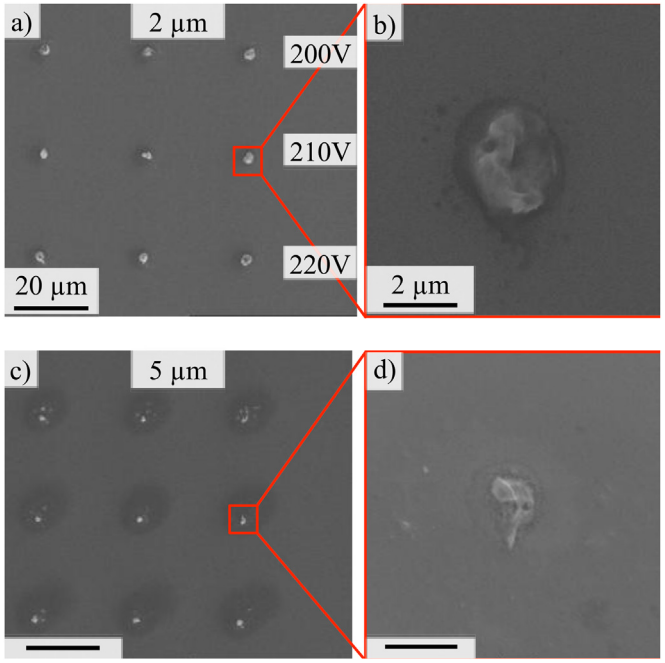

Fig. 2. Representative SEM images of ink deposited using a 1.3 µm inner diameter nozzle at a-b) 2 µm and c-d) 5 µm nozzle heights at 200 V, 210 V and 220 V for ten passes of ten 50 µs pulses with a 2 s wait time between passes. Each row has the same printing parameters. Notice that the ink sprays out over a large area (outer diameter), but accumulates into a smaller spot of silver (crystallite) when the nozzle is sufficiently close.

The graph of outer spot size vs. electric field strength in Fig. 3a shows that increasing either applied electric field strength (by increasing the applied voltage) or nozzle height increases the outer diameter. Notice that there is a distinct trend in the slopes of Fig. 3a, such that decreasing the nozzle height causes a decrease in slope. At a nozzle height of 2 µm, increasing the electric field by 40 MV/m (85 MV/m to 125 MV/m) increases the outer spot size by only 35%. In contrast, at a 10 µm nozzle height, increasing the electric field by 6 MV/m (19 MV/m to 25 MV/m) increases the outer spot size by 95%. This suggests that substrate-nozzle separation alone is not responsible for the change in $\delta D_{outer}/\delta E$ (where D is the outer diameter and E is the nominal electric field strength).

Small feature resolution is readily attained at closer nozzle heights and the E window for achieving these small spots is widened. As expected, the turn on E (*i.e.* minimum voltage to print observable deposits at a specific nozzle height) decreased with decreasing nozzle height. Fig. 2b plots the measured crystallite diameter vs. electric field strength. The larger 10 µm and 5 µm nozzle heights did not generate a distinct buildup of silver and the hollow markers denote the outer spot size under the assumption that the crystallite and outer spot sizes would be similar enough if additional passes were conducted to build up more material. For Fig. 2b, the crystallite diameter, showing the silver accumulation, does not increase with increasing electric field strength, but it does increase with increasing nozzle height.

These results are particularly interesting because it shows that outer diameter is very sensitive to the applied electric field when the nozzle is farther away from the substrate. To rule out the possibility that $\delta Q/\delta E$ (where Q is the flow rate) increases with increasing nozzle height, the volume of the deposited silver was measured using atomic force microscopy (AFM) and plotted in Figure S8 (see Supporting Information) versus the applied voltage and electric field strength. This data shows

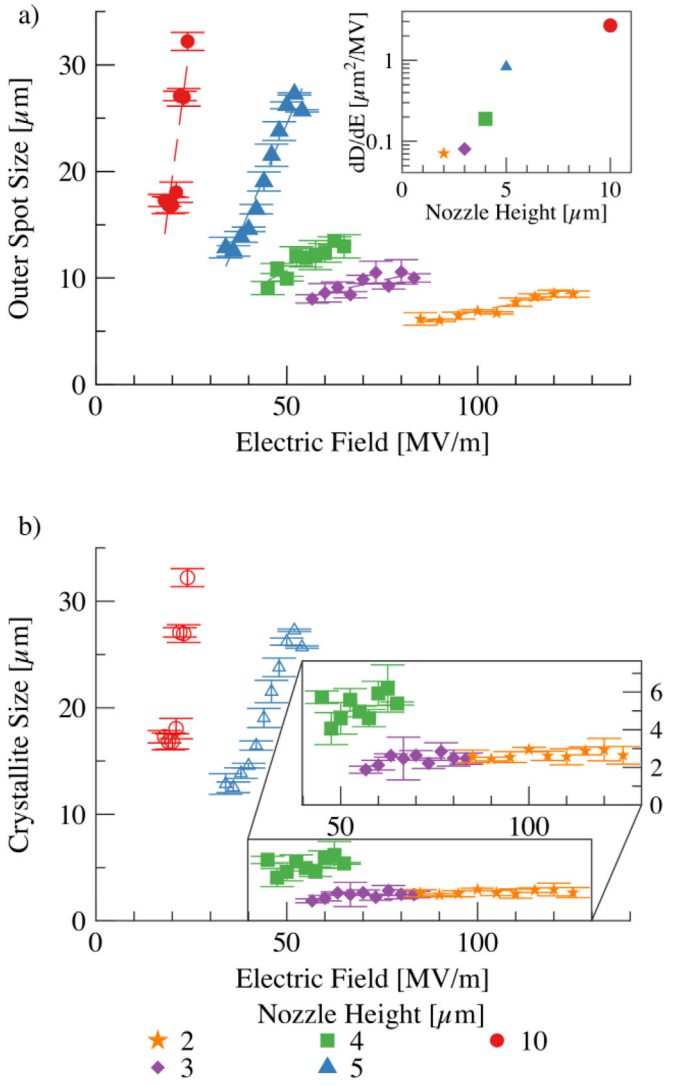

Fig. 3. Graph of the (a) outer spot size and (b) crystallite size vs. electric field strength for nozzle heights of 10 µm, 5 µm, 4 µm, 3 µm, and 2 µm. For (a), the outer spot size increases linearly with electric field strength while the slope increases with increasing nozzle height. For the crystallite size (b), no clear buildup was observed for the 5 µm and 10 µm nozzle heights and the hollow markers denote the observed outer diameter. For those nozzle heights that did form a clear buildup of silver, the crystallite diameter is independent of applied electric field.

that the deposited material volume is relatively constant for each nozzle height. A full discussion of the inconsistencies observed in deposited volume measurements is included in the Supplementary Information. Approximately, 3–4 µm [3] of material is deposited for nozzle heights of 2 µm and 3 µm and 0.5–4.5 µm [3] of material is deposited for the 4 µm, 5 µm, and 10 µm nozzle heights over the 170 V–250 V range tested.

As expected, the amount of silver deposited decreases with increasing nozzle height, supporting the idea that the observed increase in outer diameter is due breakup of the jet and an increase in the spray angle with increasing electric field strength. The plume angle can be calculated as derived by Wang et al.:

$$\tan(\theta_{plume}) = \frac{u_n}{u_a}\sqrt{\frac{3\varepsilon_0\rho_f C_\infty}{4\pi\varepsilon_l^2\rho_{e,crit}\psi_0}}\sqrt{\frac{2Q\gamma_f F z^{'}\varepsilon_0}{\psi_0\varepsilon_l\rho_f}} \tag{1}$$

where θ_{plume} is the plume angle, u_n and u_a are the normal and axial droplet velocities, ε_0 and ε_l are the vacuum and liquid permittivitities, ρ_f and $\rho_{e,crit}$ are the liquid mass and critical charge densities, C_∞ is the ionic strength, ψ_0 is the thermal potential, Q is the flow rate, γ_f is the surface tension, F is the faraday constant, and z' is the valency of an ion [13]. The distance at which the jet destabilizes is calculated according to Wang et al. as:

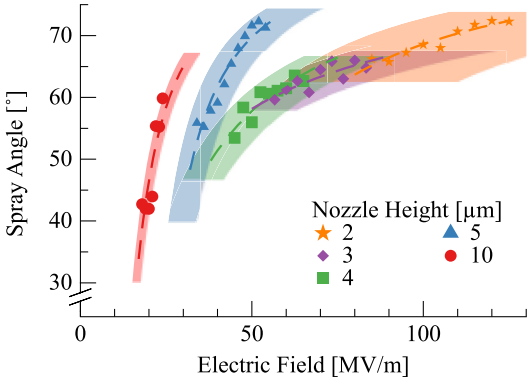

Fig. 4. Plot of observed and modeled spray angle vs. electric field for nozzle heights ranging from 2 µm to 10 µm. The banded region marks uncertainty in nozzle height due to stage drift. The good agreement between observed and modeled spray angle supports the Coulombic repulsion model.

$$L_j = (B^{-1}\psi_0\varepsilon_0^{1/2})^2\left(\ln\left(\frac{C_B}{C_\infty}\right)\right)^2\gamma_f^{-1} \tag{2}$$

where L_j is the distance to microjet breakup, B is the ratio of the inner nozzle diameter to electrode separation, and C_B is the critical surface ionic strength. Assuming a pseudo-linear approach [36] to calculate ionic strength from conductivity, $C_\infty = 0.28$ mM; B ranges from 0.2 to 1 using a nozzle height of 2 µm–10 µm and a conservative droplet size of 2 µm; the resulting distance required for the average charge separation to approach the Bjeruum length is calculated to be approximately 0 (Supporting Information). At this point, the jet undergoes Coulombic fission and the cone-jet breaks up immediately as the reactive ink exits the nozzle.

Fig. 4 plots the observed and theoretical spray angles as a function of electric field strength for the nozzle heights tested. The theoretical spray angles were fit using a reduced form of Wang et al. plume angle model by first factoring out all of the constants and assuming a theoretical cone-jet flow rate [37,38] (see Supporting Information):

$$\tan\theta = C\sqrt{\frac{V}{\ln\left(4h/r\right)}} \tag{3}$$

where V is the voltage, h is the substrate-nozzle height, r is that inner-radius of the pipette, and C is a collection of constants:

$$C = \frac{u_n}{u_a}\sqrt{\frac{3\varepsilon_0\rho_f C_\infty}{4\pi\varepsilon_l^2\rho_{e,crit}\psi_0}}\sqrt{\frac{2\gamma_f F z^{'}\varepsilon_0^2}{\psi_0\varepsilon_l\rho_f R_T r_e}} \tag{4}$$

Then, the data was fit as a function of voltage and nozzle height using Mathematica's Nonlinear Model Fit function to the form:

$$\tan\theta = C\,a\sqrt{\frac{V}{\ln\left(4h/r\right)}} + b \tag{5}$$

where the correction factors, a and b were calculated at 0.177 and −3.66 respectively. The uncertainty in nozzle height was set to ± 1 µm as the nozzle height was found to drift by this amount over the course of a day. Figure S9 shows a fit as only a function of the voltage, that provides a closer fit, but a less general result.

4. Conclusion

In conclusion, this work demonstrates that a self-reducing silver ink

can be used to fabricate fine features despite the high electrical conductivity causing breakup upon nozzle emission. A model of Coulombic repulsion was applied to ultra near-field EHD printing of highly conductive liquids to explain the observed spot size, and variations seen with changes in nozzle height and voltage. This model was validated to accurately predict deposited spot sizes at various nozzle heights by accounting for changes in plume angle as these parameters are varied. Finer resolutions would be able to be achieved through smaller nozzle heights and smaller nozzle diameters. Overall this work demonstrates that high liquid conductivity inks, specifically self-reducing silver ink, can be used to fabricate fine features with potential applications in microfluidics, plasmonics, and metamaterials.

Acknowledgements

The Authors would like to acknowledge the generous support from the National Science Foundation [NSF #1635548] and the Science Foundation Arizona [BSP 0615-15] for their kind support.

Appendix A. Supplementary data

Supplementary data to this article can be found online at https://doi.org/10.1016/j.elstat.2018.10.006.

References

[1] A. Jaworek, Electrospray droplet sources for thin film deposition, J. Mater. Sci. 42 (2007) 266–297.
[2] A. Li, Q. Luo, S.-J. Park, G. Cooks, Synthesis and catalytic reactions of nanoparticles formed by electrospray ionization of coinage metals, Angew. Chem. Int. Ed. 53 (2014) 3147–3150.
[3] S.N. Jayasinghe, A. Townsend-Nicholson, Stable electric-field driven cone-jetting of concentrated biosuspensions, Lab a Chip 6 (2006) 1086.
[4] C.H. Chen, D.A. Saville, I.A. Aksay, Scaling laws for pulsed electrohydrodynamic drop formation, Appl. Phys. Lett. 89 (12) (2006) 1–3.
[5] F.J. Higuera, Flow rate and electric current emitted by a taylor cone, J. Fluid Mech. 484 (2003) 303–327.
[6] P. Galliker, J. Schneider, H. Eghlidi, S. Kress, V. Sandoghdar, D. Poulikakos, Direct printing of nanostructures by electrostatic autofocussing of ink nanodroplets, Nat. Commun. 3 (2012) 890–899.
[7] M.W. Lee, D.K. Kang, N.Y. Kim, H.Y. Kim, S.C. James, S.S. Yoon, A study of ejection modes for pulsed-DC electrohydrodynamic inkjet printing, J. Aerosol Sci. 46 (2012) 1–6.
[8] Y.M. Shin, M.M. Hohman, M.P. Brenner, G.C. Rutledge, Experimental characterization of electrospinning: the electrically forced jet and instabilities, Polymer 42 (2001) 09955–09967.
[9] C. Wang, K.-W. Yan, Y.-D. Lin, P.C.H. Hsieh, Biodegradable core/shell fibers by coaxial electrospinning: processing, fiber characterization, and its application in sustained drug release, Macromolecules 43 (15) (2010) 6389–6397.
[10] A.J. Hijano, I.G. Loscertales, S.E. Ibáñez, F.J. Higuera, Periodic emission of droplets from an oscillating electrified meniscus of a low-viscosity, highly conductive liquid, Phys. Rev. E 91 (1) (2015) 013011.
[11] J. Kim, H. Oh, S.S. Kim, Electrohydrodynamic drop-on-demand patterning in pulsed cone-jet mode at various frequencies, J. Aerosol Sci. 39 (2008) 819–825.
[12] N.C. Schirmer, S. Ströhle, M.K. Tiwari, D. Poulikakos, On the principles of printing sub-micrometer 3D structures from dielectric-liquid-based colloids, Adv. Funct. Mater. 21 (2010) 388–395.
[13] Y. Wang, M.K. Tan, D.B. Go, H.-C. Chang, Electrospray cone-jet breakup and droplet production for electrolyte solutions, EPL-Europhys. Lett. 99 (2012) 64003.
[14] B.W. An, K. Kim, H. Lee, S.-Y. Kim, Y. Shim, D.Y. Lee, J.Y. Song, J.-U. Park, High-resolution printing of 3D structures using an electrohydrodynamic inkjet with multiple functional inks, Adv. Mater. (Weinheim, Ger.) 27 (2015) 4322–4328.
[15] J.-U. Park, M. Hardy, S.J. Kang, K. Barton, K. Adair, D.K. Mukhopadhyay, C.Y. Lee, M.S. Strano, A.G. Alleyne, J.G. Georgiadis, et al., High-resolution electrohydrodynamic jet printing, Nat. Mater. 6 (2007) 782–789.
[16] A.J. Hijano, I.G. Loscertales, S.E. Ibáñez, F.J. Higuera, Periodic emission of droplets from an oscillating electrified meniscus of a low-viscosity, highly conductive liquid, Phys. Rev. E 91 (2015) 013011.
[17] E. Castillo-Orozco, A. Kar, R. Kumar, Electrospray mode transition of microdroplets with semiconductor nanoparticle suspension, Sci. Rep. 7 (2017) 5144.
[18] L. Xu, X. Wang, T. Lei, D. Sun, L. Lin, Electrohydrodynamic deposition of polymeric droplets under low-frequency pulsation, Langmuir 27 (2011) 6541–6548.
[19] S.J.P. Kress, F.V. Antolinez, P. Richner, S.V. Jayanti, D.K. Kim, F. Prins, A. Riedinger, M.P.C. Fischer, S. Meyer, K.M. McPeak, et al., Wedge waveguides and resonators for quantum plasmonics, Nano Lett. 15 (2015) 6267–6275.
[20] J. Schneider, P. Rohner, D. Thureja, M. Schmid, P. Galliker, D. Poulikakos, Electrohydrodynamic NanoDrip printing of high aspect ratio metal grid transparent electrodes, Adv. Funct. Mater. 26 (2015) 833–840.
[21] J. Perelaer, A.W. De Laat, C.E. Hendriks, U.S. Schubert, Inkjet-printed silver tracks: low temperature curing and thermal stability investigation, J. Mater. Chem. 27 (2008) 3209–3215.
[22] A. Kamyshny, J. Steinke, S. Magdassi, Metal-based inkjet inks for printed electronics, Open Appl. Phys. J. 4 (2011) 19–36.
[23] P. Galliker, J. Schneider, D. Poulikakos, Dielectrophoretic bending of directly printed free-standing ultra-soft nanowires, Appl. Phys. Lett. 104 (2014) 073105.
[24] Y. Rosen, M. Grouchko, S. Magdassi, Printing a self-reducing copper precursor on 2D and 3D objects to yield copper patterns with 50% copper's bulk conductivity, Adv. Mater. Interfaces 2 (2014) 1400448–5.
[25] S.B. Walker, J.A. Lewis, Reactive silver inks for patterning high-conductivity features at mild temperatures, J. Am. Chem. Soc. 134 (2012) 1419–1421.
[26] Y.-C. Liao, Z.-K. Kao, Direct writing patterns for electroless plated copper thin film on plastic substrates, ACS Appl. Mater. Interfaces 4 (2012) 5109–5113.
[27] H.M. Lee, H.B. Lee, D.S. Jung, J.-Y. Yun, S.H. Ko, S. Bin Park, Solution processed aluminum paper for flexible electronics, Langmuir 28 (2012) 13127–13135.
[30] M.W. Lee, S. An, N.Y. Kim, J.H. Seo, J.Y. Huh, H.Y. Kim, Effects of pulsing frequency on characteristics of electrohydrodynamic inkjet using micro-Al and nano-Ag particles, Exp. Therm. Fluid Sci. 46 (2013) 103–110.
[31] K. Wang, J. Stark, Direct fabrication and morphology of metallic micropatterns by pulsed jet nanoelectrospraying of silver nano-ink - springer, J. Coating Technol. Res. 9 (2012) 317–322.
[32] D.K. Kang, M.W. Lee, H.Y. Kim, S.C. James, Electrohydrodynamic pulsed-inkjet characteristics of various inks containing aluminum particles, J. Aerosol Sci. 42 (2011) 621–630.
[33] S.B.Q. Tran, D. Byun, V.D. Nguyen, T.S. Kang, Liquid meniscus oscillation and drop ejection by Ac voltage, pulsed dc voltage, and superimposing dc to Ac voltages, Phys. Rev. E 80 (2009) 026318.
[34] M. GAMERO-CASTAÑO, V. HRUBY, Electric measurements of charged sprays emitted by cone-jets, J. Fluid Mech. 459 (2002) 245–276.
[35] One-dimensional simulation of the breakup of capillary jets of conducting liquids. Application to E.H.D, Spra. J. Aerosol Sci. 30 (1999) 895–912.
[36] G. Sposito, The Chemistry of Soils, second ed., Oxford University Press, New York, 2008.
[37] C.N. Ryan, K.L. Smith, J. Stark, The flow rate sensitivity to voltage across four electrospray modes, Appl. Phys. Lett. 104 (2014) 084101.
[38] C.N. Ryan, K.L. Smith, J.P.W. Stark, The influence of geometry on the flow rate sensitivity to applied voltage within cone-jet mode electrospray, J. Appl. Phys. 112 (2012) 114510.